Elsevier Editorial System(tm) for Computers in Biology and Medicine
Manuscript Draft

Manuscript Number:

Title: Simulated Temperature Distribution of the Proximal Forearm

Article Type: Full Length Article

Keywords: bio-heat equation, computer simulation, forearm temperature, Pennes' measurements, blood flow, metabolism

Corresponding Author: prof. dr. Roman Trobec,

Corresponding Author's Institution: Jozef Stefan Institute

First Author: Roman Trobec

Order of Authors: Roman Trobec; Matjaz Depolli

Abstract: Temperature changes in the resting proximal human forearm have been studied non-invasively, using computer simulation. A procedure for spatial model generation, based on digitized slice data, has been applied. A mathematical model and a 3-D computer simulation program have been implemented. Heat transfer in the non-homogenous tissue was modeled with a well known bio-heat equation. The heat production by tissue metabolism was modeled using the Q10 rule, while the heat exchange between the blood and tissue was modeled as a function of local temperature and regional blood flow. The stability and accuracy of the method was confirmed by varying the simulation parameters, the initial and boundary values, and the model dimensions, with subsequent analysis of the results.

We have explained, by computer simulation, the variations in the Pennes' well-known in vivo measurements of the steady-state temperatures along the transverse axis of the proximal forearm. Suspecting that the anatomical positioning of his measuring probes varied, we have reconstructed their possible positions by searching for the simulated positions that result in the best agreement between simulated and measured temperature fields. Our simulations indicate that the fluctuations of the measured steady-state temperatures should not be smoothed out because they are the natural consequence of a complex interplay between the position of the measuring probes, anatomical position of the main arteries, dimensions of the forearm, blood flow, inhomogeneity of tissues, and environmental temperature.

Suggested Reviewers:

Opposed Reviewers:

*Manuscript

Title

Simulated Temperature Distribution of the Proximal Forearm

Authors

Roman Trobec and Matjaž Depolli

Jožef Stefan Institute, Department of Communication Systems, Jamova 39, 1000 Ljubljana, Slovenia

Corresponding Author

Roman Trobec, e-mail: roman.trobec@ijs.si, tel: +386 1 4773 497

Abstract

Temperature changes in the resting proximal human forearm have been studied non-invasively, using computer simulation. A procedure for spatial model generation, based on digitized slice data, has been applied. A mathematical model and a 3-D computer simulation program have been implemented. Heat transfer in the non-homogenous tissue was modeled with a well known bio-heat equation. The heat production by tissue metabolism was modeled using the Q10 rule, while the heat exchange between the blood and tissue was modeled as a function of local temperature and regional blood flow. The stability and accuracy of the method was confirmed by varying the simulation parameters, the initial and boundary values, and the model dimensions, with subsequent analysis of the results.

We have explained, by computer simulation, the variations in the Pennes' well-known in vivo measurements of the steady-state temperatures along the transverse axis of the proximal forearm. Suspecting that the anatomical positioning of his measuring probes varied, we have reconstructed their possible positions by searching for the simulated positions that result in the best agreement between simulated and measured temperature fields. Our simulations indicate that the fluctuations of the measured steady-state temperatures should not be smoothed out because they are the natural consequence of a complex interplay between the position of the measuring probes, anatomical position of the main arteries, dimensions of the forearm, blood flow, inhomogeneity of tissues, and environmental temperature.

Key words

bio-heat equation, computer simulation, forearm temperature, Pennes' measurements, blood flow, metabolism

1. INTRODUCTION

The temperature of the human tissue is an important factor in many fields of physiology [1], sports [2], cryotherapy [3], etc. The temperature field is influenced by the environmental conditions, the temperatures of neighboring tissues, the muscle metabolism and the blood circulation. Different tissues have different physical and thermodynamic properties and respond diversely to temperature changes [4, 5, 6]. The temperature field varies in space and time in different parts of the investigated domain. In-vivo measurements are usually invasive and often impossible if deep tissues or vital organs are in question [7, 8].

In recent decades, computer simulations have proved a great help in understanding and solving a variety of problems in science. Especially in medicine, experiments are often difficult to perform because human subjects are involved [9]. Measurements during clinical procedures are time consuming and often not as accurate as desired, because many parameters are difficult to control [10]. In some cases, measurements during a clinical procedure would be too invasive and limited to only a few test points. An example would be a search for the highest temperature gradient in a particular part of the human body. With the use of computer simulation, however, it is possible to calculate, analyze, and visualize both stationary temperature fields and the changes of temperature in time [11].

In most scientific computing applications, a physical system is represented by a mathematical model. Real problems cannot be solved analytically, i.e., by a formula that provides the solution for any time moment and spatial point. Instead, the numerical solution must be obtained, for which the continuous physical domain has to be replaced by its discrete form. Parts of the human body are irregularly shaped three-dimensional objects, composed of different tissues, which must be represented by spatial geometric models [12]. The investigated phenomena are often described mathematically by partial differential equations (PDEs) [13].

In this paper, we applied computer simulation method, based on the well known bio-heat equation, which incorporates heat diffusion, heat generation by tissue metabolism and heat transfer between the blood and the tissue. Some important extensions have been introduced, in particular an inhomogeneous spatial

model composed of tissues with different characteristics and modeling of the heat contributions from arteries, blood perfusion, and metabolism as functions of the surrounding tissue temperature. This improved bio-heat equation was evaluated in terms of sensitivity and accuracy and solved numerically on single and parallel computers [14, 15].

The invaluable measurements of the steady-state temperature fields in forearms of unanesthetized subjects, published by Pennes, sixty years ago [9] have still not been explored in all details [16]. We see from Figure 1 that the author tries to smooth the discrete measurements. We have shown that this is inappropriate because local gradients in the temperature profiles have biological background.

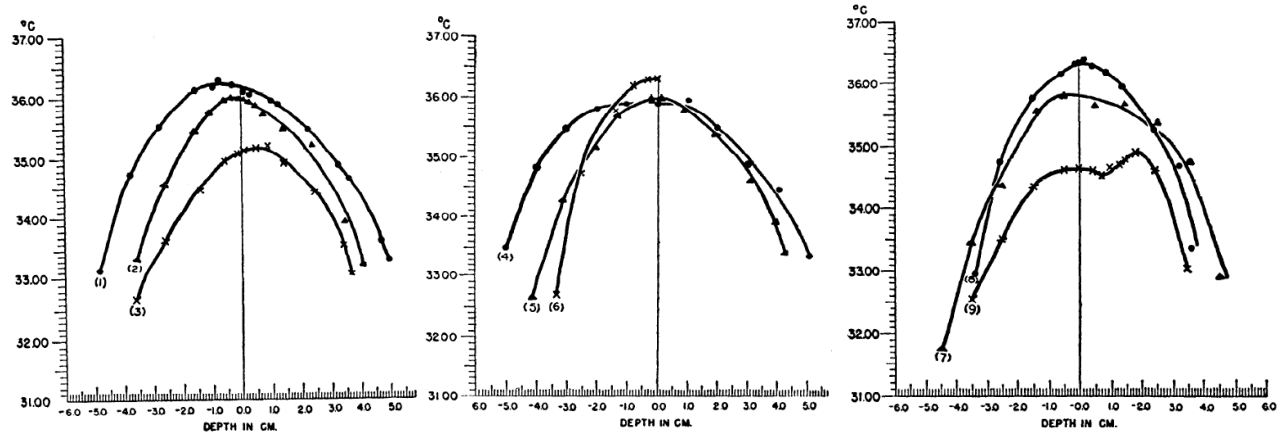

Figure 1. The steady-state temperature profiles in forearms of nine unanesthetized subjects, as appeared in the original Pennes' publication [9].

Other experimental data are available for the temperature of the forearm during an immersion in water of various temperatures, either as it evolves in time [17] or near its steady-state [4]. These measurements have since been elaborated by others [18, 19]. In some recent studies, measured temperature profiles in forearm cross-sections are reported, together with estimated values for the in-vivo thermal conductivities of muscle and subcutaneous tissues [19], but with lower resolution than in Pennes' paper. We have recreated in simulation the conditions similar to those of the Pennes' measurements, and have simulated the steady-state temperatures of the proximal forearm. Our simulation methodology proved adequate in explaining most of the fluctuations in Pennes' measurements through the position of the measuring probe, the diameter of the subject forearm, the vicinity of arteries, and the inhomogeneities of the tissues.

The rest of the paper is organized as follows. In the next section the spatial forearm model is described. Different simulation modalities and parameters are then presented, followed by a description of the

mathematical model. The solution method is described, together with a conceptual description of the computer program for the numerical simulation. Section 3 is devoted to presentation and analysis of the simulated results and their comparison with the measured values. The simulation methodology is confirmed to be robust by the analysis of its sensitivity. In the Discussion, different aspects of the proposed methodology are mentioned, which have been inspired by the simulated results. Limitations of the proposed methodology are also stressed. The paper concludes with a short summary and some directions for future work.

2. METHODS

2.1. Geometric Model of the Forearm

The basic anatomical data for a computer model of the forearm was derived from the digital photographs of the human body cross-sections (thorax 1601 – 1800), each 1 mm apart, that are available from the Visible Human Dataset (VHD) [20] with a resolution of 0.33 mm in the X-Y (transversal) plane. The cross-sections corresponding to the right forearm section were cropped from the original photographs as rectangles of 506 (width) × 632 (height) pixels. The VHD right forearm is inclined by 32.5º in the X-Z (coronal) plane and by 43.1º in the Y-Z (sagittal) plane. Because the measuring position of the Pennes' measuring probe was transversal to the forearm axis, the cropped VHD cross-sections were rotated in 3-D by the above angles, to obtain 100 transversal slices of the forearm segment, shown in Figure 2. The slices obtained after rotation have been further cropped to the dimensions of 420 × 348 pixels. The rotated and cropped slices are termed as 'model slices' in the rest of the paper. The positions of different tissues, e.g. muscles, bones, subcutaneous tissue, skin, nerves, veins and arteries were determined manually, using an open source visualization program [21], and assisted by an expert anatomist.

The 3-D geometric model was built simply by stacking the 100 model slices, generating a model of a section of the human forearm, 50 mm distal to the tip of the elbow and 100 mm long. Because at the original resolution, the total number of pixels was too large for a full 3-D simulation, and the axial distance between neighboring slices was already 1 mm, we reduced the model slices resolution to 1 mm too, by averaging 9 neighboring pixels on a slice and merging them into one. Thus we created a 3-D geometric model of the forearm, composed of $X \times Y \times Z = 140 \times 116 \times 100 = 1{,}624{,}000$ small cubic volume elements (voxels) with 1mm edges, shown in the right side of Figure 2. For better visibility of the bones and arteries in the model, muscles, skin and subcutaneous tissues are shown semi-transparent.

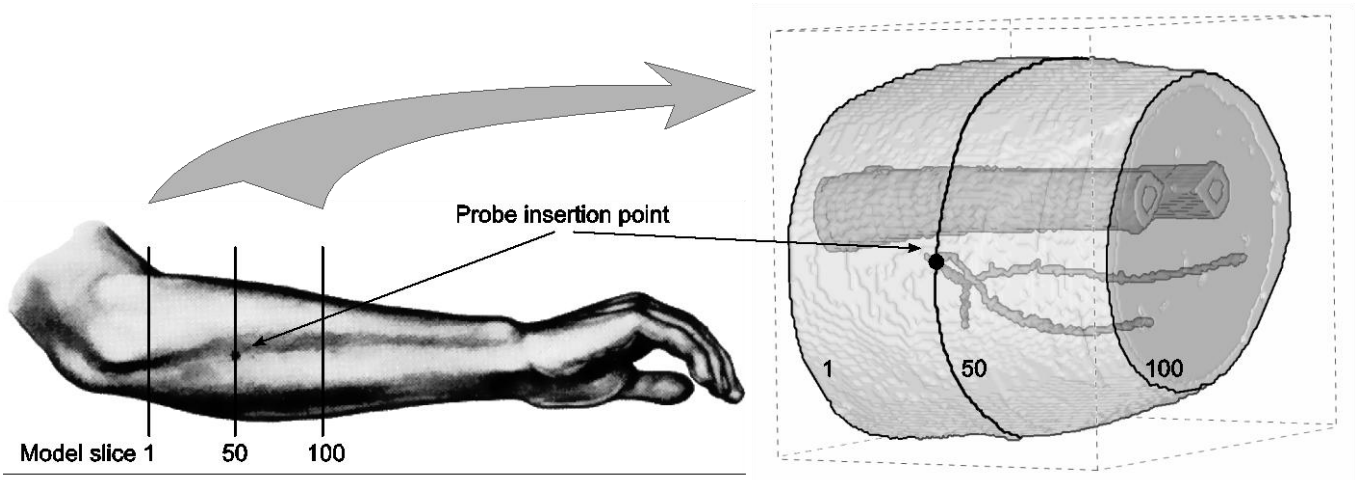

Figure 2. Right human arm in the position as measured by Pennes (left). 3-D model of the simulated forearm part (right) with labeled model slices 1, 50, and 100. On the model, two bones (radius behind ulna) along with the ulnar and radial arteries are shown through the semi-transparent muscles, subcutaneous tissue and skin.

In Figure 3 model slice 50 is shown with different tissues labeled and marked by different levels of gray. Horizontal measuring axis and points of interest, used later in this paper, are labeled by arrows and (X, Y) coordinates. There is a small amount of unlabeled adipose tissue around the arteries and nerves, and above the bones; only the cephalic vein is labeled from the modeled set of veins; the border between the cortical and cancellous bone tissues is marked by a thin line.

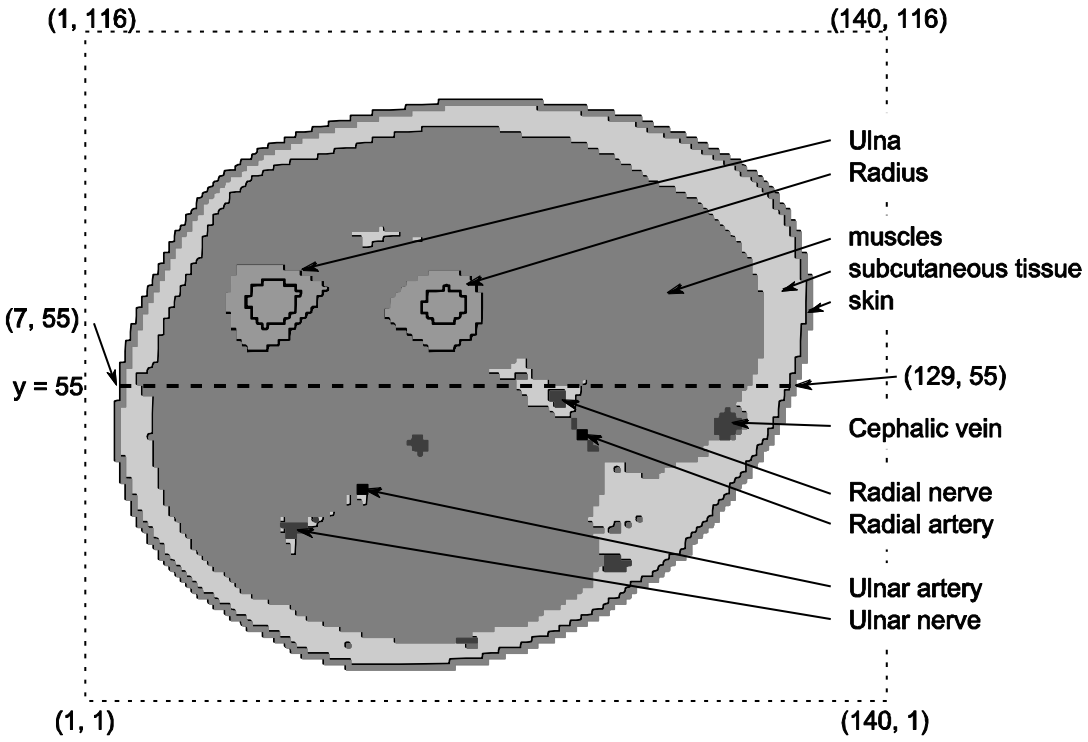

Figure 3. Model slice 50 at a resolution of 1 mm. Different tissues are marked by different levels of gray. Model slice corners and other points of interest are labeled by pixel coordinates. Horizontal line at Y=55 marks the approximate path of the Pennes' thermocouple probe.

Pennes measured forearms with significantly different diameters (7 – 10 cm) at "8 cm distal to tip of ulna olecranon" [9] – or 8 cm from the tip of elbow. In the case that 8 cm were strictly respected, the variation in the position of the measuring probe, regarding the forearm anatomy, could be significant − up to 25% of the distance to the elbow.

The diameter of the described geometric model of the forearm at slice 50, which is in the middle of the model, is 12.4 cm. To obtain a closer match to the measured forearms, which were significantly smaller, we linearly scale the geometric model, to a desired diameter. In the rest of the paper, we use the diameter of 8.3 cm except when we explicitly specify it otherwise. Scaling works directly on dimensions of voxels, therefore keeping the number of voxels in the model unchanged, while changing the model dimensions.

2.2. Simulation Parameters

Thermal Constants

Numerical values of thermal constants for living tissues are not known precisely, because, for example, they depend on the tissue temperature. Also the measuring equipment and method used could introduce a significant variance [22, 23]. We determined the thermal constants as an average of published data [18, 24, 25, 26]. Each voxel of the geometric model is characterized by constant coefficients – heat conductivity λ, specific heat c, and density ρ, which are often combined into thermal diffusivity D, where $D=\lambda/c\rho$ (see Table 1).

Blood Flow

Published measurements of the blood flow rate show that the blood flow increases with the tissue temperature [19, 27]. Earlier measurements of the forearm blood flow were limited to the plethysmography, which measures the mean total blood flow through a given region of the forearm [28], later more data became available also for regional blood flow of specific tissues [29, 30, 31]. Several studies have established that the muscle blood flow does not increase with increasing temperature; most of the increase takes place in the skin [32].

The mean forearm blood flow rate V was modeled as a function of skin temperature T_s, which was obtained by fitting the published experimental data [17, 27, 29, 33, 34] with exponential function:

$$V(T_s) = (5.142\ 10^{-5}\ e^{0.322\ Ts} + 0.705)\ \text{ml}\ (100\ \text{ml})^{-1}\ \text{min}^{-1}, \qquad (1)$$

which results, for example, in $V(33\ ^{o}\text{C}) = 2.8$ ml $(100$ ml$)^{-1}$ min^{-1} or $4.7\ 10^{-4}$ s^{-1}. We separated the total blood flow into regional blood flows for each tissue and modeled the regional blood flow rate $V_r(T)$ with the same exponential function as in Equation (1), substituting T for T_s:

$$V_r(T) = v_r\ V(T), \qquad (2)$$

The dimensionless regional blood flow rate fraction v_r was introduced to allow for different blood flow rates in different tissues. v_r were determined based on the measured ratios between blood flow rates in different tissues [29, 30, 31]. The values of v_r were obtained by an iterative procedure, to maintain the mean forearm blood flow rate V from Equation (1). First, initial approximations of v_r were used for the simulation of a medium sized (diameter of 8.3 cm) forearm resting at an ambient temperature of 25 °C. From the obtained temperature field, the regional blood flow rates $V_r(T)$ and their mean were calculated. The mean $V_r(T)$ should equal the mean forearm blood flow rate $V(T_s)$, where T_s is the mean skin

temperature obtained by the simulation. After comparing the simulated $V_r(T)$ with $V(T_s)$, the eventual difference was reduced by multiplying all the values of v_r by a factor of $V(T_s)/V_r(T)$, thus preserving the ratios between v_r. Then, because the values of v_r influence the simulated temperature field, the whole process was repeated until the desired accuracy of mean $V_r(T)$ was achieved.

We considered the steady-state of the forearm and have therefore not incorporated the autonomic thermoregulation (vasodilatation, vasoconstriction), as we assumed that their effects are stable when the forearm is at rest and its temperatures do not change with time. Although a more detailed blood flow model could be used in our simulation, its development is beyond the scope of our paper.

Metabolism

Metabolic heat production in the human can be separated into unregulated heat production from voluntary muscle contraction and normal metabolic pathways, and into regulated heat production for maintaining temperature homeostasis at lower ambient temperatures [6, 35]. The rate of metabolic heat production per unit mass h_m was assumed to obey the Q_{10} rule [36], which is expressed as a function of the tissue temperature:

$$h_m(T) = h_r\, 2^{(T-Tr)/10}, \qquad (3)$$

where h_r is the reference metabolic heat production of a tissue at reference temperature T_r = 35 ºC. For muscles at rest, h_r was taken to be about half the human basal metabolic rate, which equals 0.6 W kg^{-1} [2, 37, 38]. The impact of the metabolic rate production is almost negligible for the temperature field in the forearm; even so, it can be adjusted in the model for each tissue independently. We derived the values from the available data in the literature listed above.

The thermal constants, regional blood rate fractions and reference metabolic heat production used in the simulation, are listed in Table 1.

Table 1. Simulation parameters

	λ [Wm^{-1} ºC^{-1}]	c [J kg^{-1} ºC^{-1}]	ρ [kg m^{-3}]	v_r	h_r [W kg^{-1}]
Skin	0.51	3431	1200	0.4	0.3
Subcutaneous/adipose tissue	0.55	2241	812	0.4	0.3

Muscle	1.03	4668	1179	0.8	0.6
Cortical bone	2.28	1260	1700	0.2	0.1
Cancellous bone	0.5	2260	900	0.6	0.3
Nerve	0.5	3277	1190	1.1	0.3
Blood	0.67	3890	1057	/	/
Ambient air	0.025	1012	1.29	/	/
Water	0.58	4204	1000	/	/

2.3. Mathematical Model

Because the human forearm is an irregularly shaped three-dimensional object, it cannot be represented as a combination of simple geometric objects and its temperature distribution cannot be obtained analytically. The temperature change rate was modeled by a partial differential equation of the second order, based on the well known bio-heat equation [9, 39]:

$$\frac{\partial T}{\partial t} = D\nabla^2 T + \frac{\rho_b c_b}{\rho c} V_r(T)(T_a - T) + \frac{1}{c} h_m(T), \qquad (4)$$

where T is the temperature of a tissue, t is time, ρ_b and c_b are the density and specific heat of blood, and all other notations are as defined previously. Besides the diffusion, Equation (4) also models the heat transfer between the arterial blood and tissues, and the heat production arising from tissue metabolism, which are separately shown, for muscle, in Figure 4. The contribution of metabolism is minimal, while the blood perfusion acts as a heat source, at temperatures lower than T_a. However, if the tissue temperature rises above T_a, the arterial blood effectively cools the tissue [40, 41]. The behavior of other tissues differs only for a constant factor.

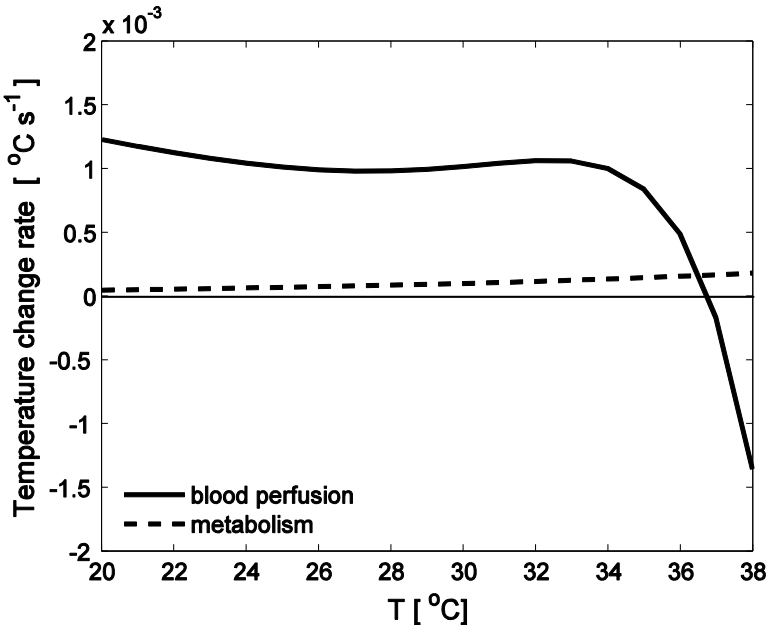

Figure 4. The modeled temperature change rate caused by the blood perfusion and metabolism as a function of muscle temperature.

2.4. Numerical Solution

We selected the Explicit Finite Difference Method (EFDM) for the numerical solution procedure [13], because it has low calculation complexity, is sufficiently accurate, and is simple to implement [42]. In addition, EFDM can directly use the available geometric model as its discretized domain. Although we are currently only interested in stationary temperature field of the domain, EFDM can also be used to determine the evolution of the temperature of different tissues in the domain for the analysis of time dependent problems.

We simulated the steady-state temperatures of the resting forearm near the thermo-neutral conditions. It is known that the thermo-neutral conditions of an unclothed arm with skin temperature of 33 °C are obtained at the ambient air temperature of 25.2 ± 1.1 ºC [5]. The initial conditions of our simulation comprise the temperatures of all the modeled tissues except arteries, and are all set to 36 ºC. The temperatures of the arteries, which act as heat generators, and ambient air, which acts as heat sink, form the boundary conditions of the simulation, and are set to constant 36.8 ºC and 26 ºC, respectively. After running the simulation, the tissue temperatures converge towards their stationary values. In our case, the near steady-state was reached after three simulated hours, with the maximal changes of temperatures in the last hour 0.01 ºC and with the skin surface temperature 33 °C.

Moving air was not simulated because of its significant contribution to the calculation complexity [43]. We simulated the heat flow between the skin surface of the forearm and the ambient air using convective boundary conditions [44], based on the continuity of the heat flow perpendicular to the surface of the simulated body part:

$$\lambda \frac{\partial T}{\partial n} = H(T_a - T). \qquad (5)$$

In the equation, T_a and T are ambient and boundary voxel temperatures, respectively. The convection coefficient H = 16 W m^{-2} $^oC^{-1}$ was determined by numerical experiments, based on the simulation of the thermo-neutral conditions (T_a = 26 ºC, T_s = 33 ºC), maintained also by Pennes' measurements. $\frac{\partial}{\partial n}$ denotes derivative along the outward normal to the face of the surface voxel, which is in contact with air. As seen from the Figure 3, contact surfaces between the skin and air are not smooth as a consequence of an equidistant orthogonal discretization. Therefore, a surface smoothing was implemented on the voxels of the model that are in contact with air. The surface smoothing keeps the contact areas of surface voxels with a single face in contact with air unchanged – 1 mm^2. For surface voxels with 2, and 3 or more faces in contact with air, their contact surface areas are reduced to $\sqrt{2}$ mm^2 and 2 mm^2, respectively. This method was experimentally evaluated and proved to provide errors less than 0.01 ºC, which is sufficiently accurate for our simulation.

The influence of the parts of the forearm that were not simulated, was mimicked by setting the heat flow to zero at both "ends" of the modeled arm (slice 1 and 100) indicating a thermal equilibrium between the modeled and excluded parts of the forearm.

3. RESULTS

3.1. Steady-state Forearm Temperature Profiles

The simulated steady-state temperature field of the model slice 50 with the diameter of 8cm after three hours of simulation is shown in Figure 5a. The impact of each of the two main arteries (ulnar and radial), with constant blood temperature, is visible as peaks in the temperature profile at the locations of the arteries, which are marked by the two vertical lines. We can also notice that the skin temperature depends on the position because its distance from the arteries varies. The steady-state temperature profile taken from the same slice along the path of the Pennes' thermocouple measurements (referred to as the

measurement path in the rest of the paper) is shown in Figure 5a by a white curve and also in Figure 5b by a thick solid curve. The dotted curve shows the analytical solution of the bio-heat equation [1] for a cylindrical homogeneous model with blood flow $V = 4.7\ 10^{-4}\ s^{-1}$, $h_m = 0.62\ J\ kg^{-1}s^{-1}$, skin temperature $T_s = 32.5\ ^oC$ and with other constants ρ_b, c_b, and T_a, set the same as in the simulation. We see that the analytical solution of the homogenous model can reproduce the general trends in the temperature gradients; however, it cannot reproduce the measured results because it is symmetric and uniform throughout the model.

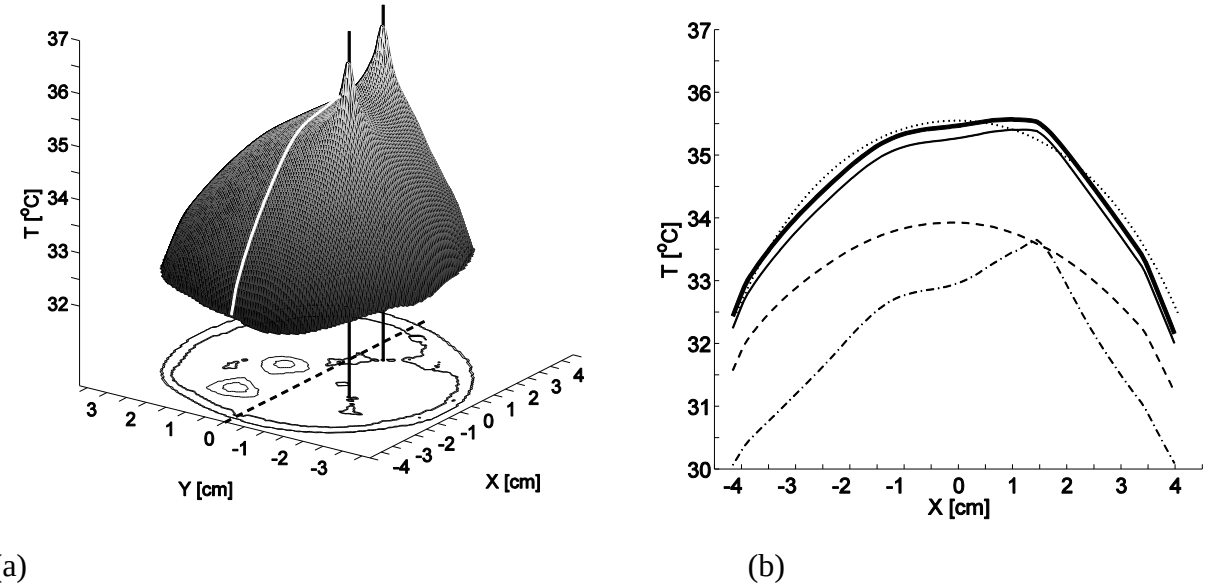

(a) (b)

Figure 5. (a) Model slice 50 and its steady-state temperature field. The simulated temperature profile along the approximate measurement path (dashed line) is emphasized with a white line. The positions of two main arteries are marked by vertical lines. (b) Simulated temperature profiles along the same path as in (a). The unmodified profile (thick curve) is contrasted against the analytical solution of the bio-heat equation on a homogenous cylindrical model (dotted curve) and the profiles acquired with modified simulation: disabled metabolism (solid thin), arteries not a heat source (dashed), and disabled blood perfusion (dashed/dotted).

By disabling, one at a time, the metabolism, main arteries, and blood perfusion in the simulation, we obtain the last three temperature profiles shown in Figure 5b. The thin solid curve shows the simulated temperature without metabolism. We can see that the metabolism minimally contributes to the final temperature. The dashed curve was obtained by not keeping the arteries at a constant temperature in the

simulation, thus canceling their heat generating role. The impact of the arteries not heating up the surrounding tissue makes this temperature profile stand out among the simulated profiles by having lower than normal deep muscle temperature and being more symmetric. The dashed/dotted curve, obtained by the simulation with the arteries at a constant temperature T_a and disabled blood perfusion, confirms that the contribution of the blood perfusion is essential. The average temperature of this profile is significantly lower with pronounced peaks corresponding to the two main arteries.

3.2 Sensitivity Analysis

The simulated steady-state solution was evaluated regarding its sensitivity. Input parameters were varied within the selected ranges and the variations in the resulting temperature profiles were analyzed. In Figure 6 the simulated temperatures from model slice 50 along the measurement path are shown, after three hours of the simulated resting forearm, exposed to ambient air at 26 ºC, with varying forearm diameter, thermal diffusivity, blood flow, and metabolism, all for +20% (dotted line) and -20% (dashed line) of their nominal values (solid line). A slight exception of this rule is Figure 6a, where instead of the nominal value, a 10 cm diameter is taken as the central value.

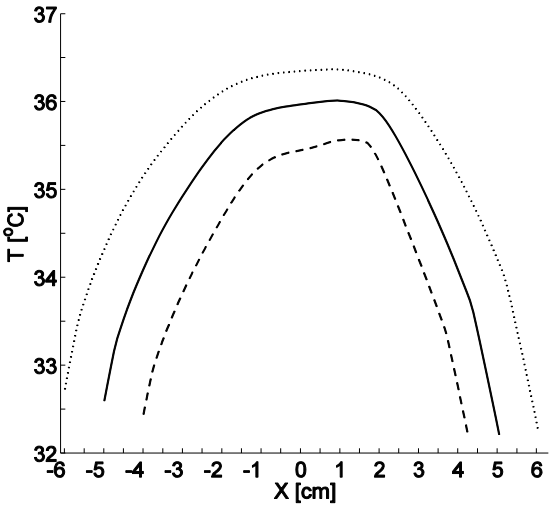

(a)

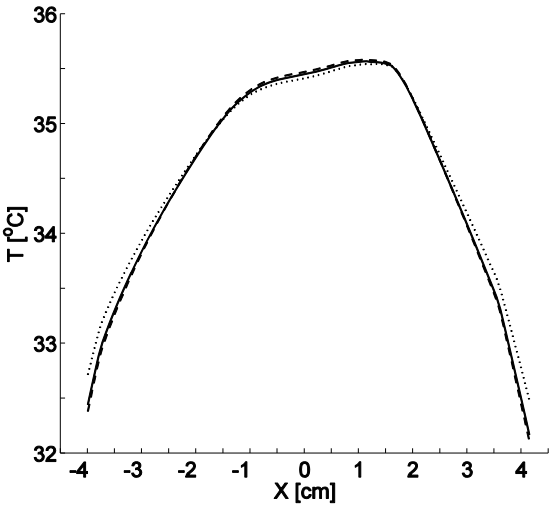

(b)

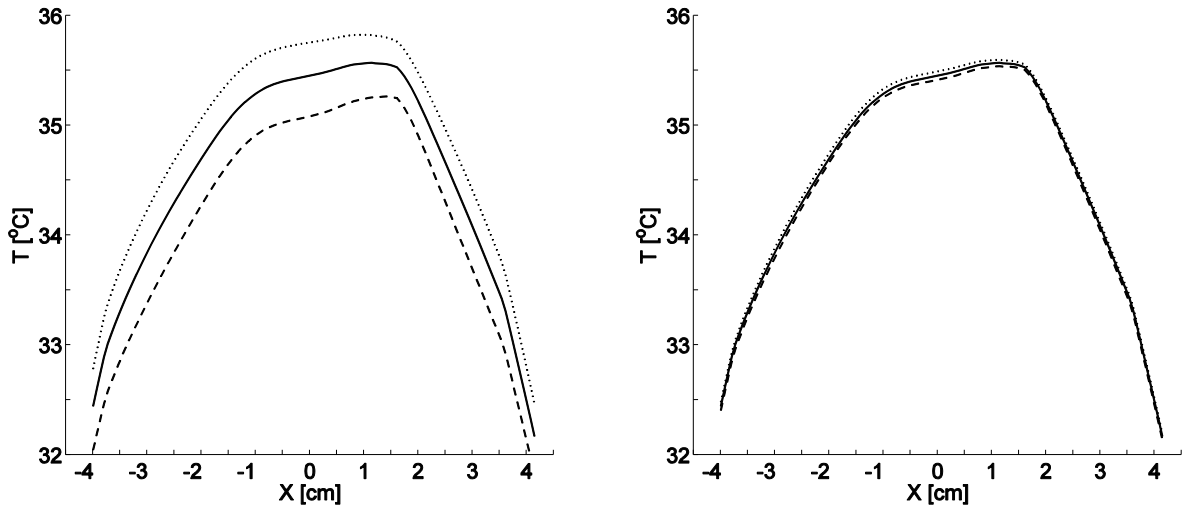

(c) (d)

Figure 6. Simulated temperatures from the model slice 50 along the measurement path after simulated three hours resting forearm at a room temperature of 26 ºC for various: (a) forearm diameters, (b) thermal diffusivity, (c) blood flow, and (d) metabolism. All panels feature solid, dotted, and dashed lines for the results acquired using the nominal, 20% above nominal, and 20% below nominal values of the given parameter, respectively.

The most significant impact on the temperature profiles comes from varying the forearm dimension (Figure 6a). The largest arms result in a plateau slightly above 36.3 ºC, while the smallest arms are cooled more intensively reducing the maximal temperature to 35.6 ºC, with larger temperature gradients in the superficial regions of the forearm. Changes in the thermal diffusivity (Figure 6b) have a much smaller impact on the temperature profiles as the forearm dimension. The effect is also non uniform across the profile, but is rather equalizing the superficial and the deep muscle temperatures. The impact of the blood flow (Figure 6c) is again uniform across the profile, with higher forearm temperatures when the blood flow is larger. The impact of the metabolism is analogous to that of the blood flow − greater metabolism results in higher forearm internal temperatures − but significantly smaller in scale.

3.3. Reproducibility of Pennes' Measurements

Pennes described in his famous paper [9] the different sources of measuring errors. The positions of measuring points and the reading of temperature values have been of limited accuracy, which could

result in errors of 0.1 ºC. The dimensions of thermocouples were up to 0.2 mm and hence in the areas of steepest temperature gradient, near the forearm surface, an additional error could be introduced.

To reproduce the Pennes' measurements we first simulated the resting forearms under the same conditions and environment, as in real measurements. Then we have applied a search, over the simulation results, for the optimal simulated positions of measuring probes that result in the best fit to the measured temperature profiles. To assess the differences between the simulated and measured profiles, we used the root mean square (RMS) error, weighted with Gaussian function, to diminish the effect of greater inaccuracies in measurements near the forearm surface. The similarity between the measured profiles and the simulated profiles that fit them best is given by Pearson correlation coefficient for all analyzed measurements in Table 2. The simulated paths of the measuring probes, which provide the highest correlation between the simulated and measured profiles, are also determined in Table 2 by two offsets and two angles to the measurement path. They can be obtained by applying sequentially the translations in Y and X directions and rotations in X-Y and X-Z planes to the path of the Pennes' thermocouple probe.

Table 2. Comparison between the measured forearm temperature profiles and simulated temperature profiles that fit them best, for all analyzed measurements

	Subject							
	1	2	3	4	5	7	8	9
Correlation	0.988	0.995	0.993	0.980	0.997	0.989	0.980	0.991
Y offset [mm]	-2.6	2.7	4.5	1.8	5.7	-0.4	2.4	1.2
Z offset [mm]	-21.4	-32.7	-30.3	-9.3	-28.8	-9.0	-36.3	-4.4
Angle in X-Y plane [°]	0	-0.4	-1.6	-0.4	0	0.4	0	3.5
Angle in X-Z plane [°]	5.5	5.9	0	0.8	7.8	4.3	3.9	4.3

Two typical simulated temperature profiles are shown in Figure 7, together with measured points. The central peak in the profile of measurement 4 is expected and can also be predicted by the theory. The temperature profile of measurement 9 with dual maxima can be explained by the probe moving close to and about the same distance from both arteries. The left and right shifted maxima visible in some other measurements can be explained by the path of the temperature probe being closer to either ulnar or radial artery. The difference in forearm dimensions result in significantly different temperatures in the central part of the forearm. As visible from Figure 7, larger forearms induce higher temperatures.

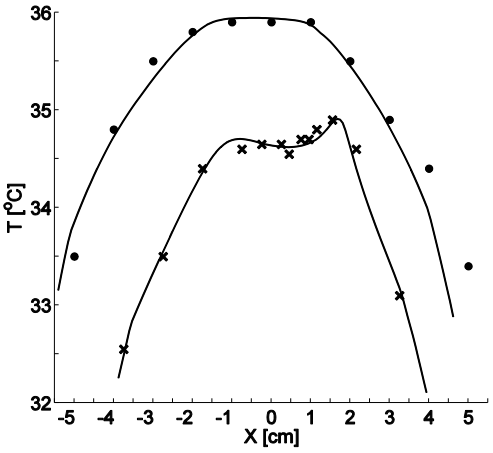

Figure 7. The best fit of the simulated temperature profiles (solid curves) to Pennes' measurements for subject 4 (circles) and subject 7 (crosses) obtained by searching for the optimal position of the simulated measuring probe.

4. CONCLUSION

Our primary goal was to explain, by computer simulation, the variations in the Pennes' well-known in vivo measurements of the steady-state temperatures along the transverse axis of the proximal forearm. Suspecting that because of the different forearm sizes of the subjects, the anatomical positioning of the measuring probes varied, we have reconstructed their possible paths by searching for the simulated paths that result in the best agreement between simulated and measured temperature fields. Several attempts have been made in the past to average the measured steady-state temperatures in order to smooth fluctuations and obtain a standardized response. Our simulated results suggest that this approach is inappropriate. Our simulations indicate that such fluctuations are natural results and the consequence of a complex interplay between the position of the measuring probe, anatomical position of the main arteries, dimensions of the forearm, blood flow, inhomogeneity of tissues, and environmental temperature.

In our endeavor to extract as much information from the existing measurements as possible, we have developed several innovative approaches in the simulation method. A procedure for spatial model

generation based on digitized slice data has been developed. A mathematical model and a 3-D computer simulation program have been implemented for the simulation of steady-state temperatures of human forearm. Heat transfer in the model with non-homogenous tissue was modeled with a well-known bio-heat equation. The heat production by tissue metabolism was modeled using the Q10 rule, while the heat exchange between the blood and tissue was modeled as a function of local temperature and regional blood flow, which in turn was modeled as an exponential function fitted to experimental data. The regional blood flow was assumed to depend on the regional temperature in the same way as the mean blood flow rate depends on the skin temperature. Such an approach produced reasonable results, nevertheless, it needs to be supported by further physiological research. The developed simulation, however, is sufficiently robust to incorporate arbitrary model functions for blood flow and metabolism. The stability of the method was confirmed by varying simulation parameters, initial and boundary values, and model shape, with subsequent analysis of the results.

We have confirmed that blood flow has a significant and complex impact on the steady-state temperatures of the forearm. Lower blood flow results in the lower temperature of the central part of the forearm. When the effect of blood flow on the temperature profile is increased, by disabling the direct effect of the main arteries, the resulting temperature profiles match very well the analytically produced profiles from the literature, but not well with the experimental measurements. We have shown that only when the effect of both, the heat distributed via blood flow, and the heat emitted directly from the arteries are considered, the measured temperature profiles can be fully explained. Furthermore we have revealed the dependence of the temperature profile shape on the dimensions of the forearm. Smaller forearms are more likely to feature off-center peaks in the vicinity of main arteries than larger forearms in which a central plateau may form, masking all other potential peaks. The thermodynamic constants of the tissue and the tissue metabolism were confirmed to have a relatively minor impact on the temperature field.

The presented methodology has several limitations. It was previously validated on the case of a cooling human knee [45], which has a different proportion of the constituent tissues and distribution of the main vessels. In vivo validation on the forearm, however, is not applicable. The anatomy of the forearm differs between individuals and changes in time, and consequently the simulation on one generalized model can differ from the experimental measurements. Minor errors in tissue segmentation and inaccurate thermodynamic constants could also produce small errors in the simulated results. The possible influence of different mechanisms of thermoregulation on blood perfusion has not been simulated because we assumed that their effects are stable when the forearm temperature is in its steady-state. If required, these

mechanisms could be easily incorporated into the simulation. Although all these limitations of the model could have some impact on the simulated temperatures, the essential findings are in close agreement with in vivo measurements, particularly if the inaccuracy of the position of the measuring path is accepted.

The long run times of the presented 3-D simulation constitute a technical limitation. The initial simulations were therefore done in 2-D on a single model slice, with the heat flux in the axial direction set to zero, emulating an infinitely long "forearm" with homogenous structure in the axial direction. Although the 2-D simulation times were shorter by several orders of magnitude, there were minor differences in the steady-state temperature profiles. The results presented in this paper have been obtained by the 3-D simulation.

Future work includes the simulation of the temperature field evolution in time and analysis of the possible impact of the measuring probes, surgical instruments and other medical equipment on the temperature fields. Using an approach analogous to that presented here, other parts of the human body could also be simulated and their temperature fields analyzed. The spatial forearm model and simulation program are available for research purposes from the corresponding author.

Acknowledgement

The authors acknowledge the financial support from the state budget by the Slovenian Research Agency under grant P2-0095.

REFERENCES

1. F. Yamazaki, R. Sone. Modulation of arterial baroreflex control of heart rate by skin cooling and heating in humans, *J Appl Physiol* 88: 393–400, 2000.
2. S. S. Ho, M. N. Coel, R. Kagawa, A. B. Richardson. The effects of ice on blood flow and bone metabolism in knees, *Am J Sports Med* 22: 537–40, 1994.
3. S. S. Martin, K. P. Spindler, J. W. Tarter, K. Detwiler, H. A. Petersen. Cryotherapy: an effective modality for decreasing intraarticular temperature after knee arthroscopy, *Am J Sports Med* 29: 288–291, 2001.
4. K. Aoki, N. Kondo, M. Shibasaki, S. Takano, T. Katsuura. Circadian variation in skin blood flow responses to passive heat stress. *Physiology & Behavior* 63: 1–5, 1998.

5. M. B. Ducharme, W. P. VanHelder, M. W. Radomski. Tissue temperature profile in the human forearm during thermal stress at thermal stability. *J Appl Physiol* 71: 1973–1978, 1991.
6. C. I. Proulx, M. B. Ducharme, G. P. Kenny. Effect of water temperature on cooling efficiency during hyperthermia in humans. *J Appl Physiol* 94: 1317–1323, 2003.
7. B. Karaszewski, J. M. Wardlaw, I. Marshall, V. Cvoro, K. Wartolowska, K. Haga, P. A. Armitage, M. E. Bastin, M. S. Dennis. Measurement of brain temperature with magnetic resonance spectroscopy in acute ischemic stroke. *Ann Neurol* 60: 438–446, 2006.
8. M. Šterk, R. Trobec. Biomedical simulation of heat transfer in a human heart. *J Chem Inf Mod* 45: 1558–1563, 2005.
9. H. H. Pennes. Analysis of tissue and arterial blood temperature in the resting human forearm. *J Appl Physiol* 1: 93–122, 1948.
10. M. Antonic, B. Gersak. Renal function after port access and median sternotomy mitral valve surgery. *Heart Surgery Forum* 10: E401–E407, 2007.
11. J. Werner, M. Buse. Temperature profiles with respect to inhomogeneity and geometry of the human body. *J Appl Physiol* 65: 1110–1118, 1988.
12. D. A. Nelson, S. Charbonnel, A. R. Curran, E. A. Marttila, D. Fiala, P. A. Mason, J. M. Ziriax. A High-Resolution Voxel Model for Predicting Local Tissue Temperatures in Humans Subjected to Warm and Hot Environments. *J Biomech Eng* 131: 041003 (12 pages), 2009.
13. M. N. Özisik. *Finite Difference Methods in Heat Transfer*. Boca Raton: CRC Press, 1994.
14. S. G. Akl. *Parallel Computation: Models and Methods.* New Jersey: Prentice Hall, 1997.
15. R. L. Martino, C. A. Johnson, E. B. Suh, B. L. Trus, T. K. Yap. Parallel computing in biomedical research, *Science* 265: 902–908, 1994.
16. E. H. Wissler. Pennes' 1948 paper revisited. *J Appl Physiol* 85: 35–41, 1998.
17. H. Barcroft, O. G. Edholm. Temperature and blood flow in the human forearm. *J Physiol* 104: 366–376, 1946.
18. H. F. Bowman, E. G. Cravalho, M. Woods. Theory, measurement, and application of thermal properties of biomaterials. *Annu Rev Biophys Bioeng* 4: 43–80, 1975.
19. M. B. Ducharme, J. Frim. A multicouple probe for temperature gradient measurements in biological materials. *J Appl Physiol* 65: 2337–2342, 1988.
20. M. J. Ackerman. The visible human project. *Proc IEEE* 86: 505–511, 1998.
21. GNU Image Manipulation Program – GIMP. Available on http://www.gimp.org/.
22. T. E. Cooper, G. J. Trezek. Correlation of thermal properties of some human tissue with water content. *Aerosp Med* 42: 24–27, 1971.

23. S. R. H. Davidson, D. F. James. Measurement of thermal conductivity of bovine cortical bone. *Med Eng & Physics* 22: 741–747, 2000.

24. W. M. Moses, G. L. Geddes. Measurement of the thermal conductivity of equine cortical bone. American Society of Mechanical Engineers, *BED* 17: 185–188, 1990.

25. E. Ponder. The coefficient of thermal conductivity of blood and various tissues. *J Gen Phisiol* 45: 545-551, 1962.

26. H. F. Poppendiek, R. Randall, J. A. Breeden, J. E. Chambers, J. R. Murphy. Thermal conductivity measurements and predictions for biological fluids and tissues. *Cryobiology* 3: 318–327, 1967.

27. C. B. Wenger, L. A. Stephenson, M. A. Durkin. Effect of nerve block on response of forearm blood flow to local temperature. *J Appl Physiol* 61: 227–232, 1986.

28. H. Barcroft, O. G. Edholm. The effect of temperature on blood flow and deep temperature in the human forearm. *J Physiol* 102: 5–20, 1943.

29. K. E. Cooper, O. G. Edholm, R. F. Mottram. The blood flow in skin and muscle of the human forearm. *J Physiol* 128: 258–267, 1955.

30. E. C. McElfresh, P. J. Kelly. Simultaneous determination of blood flow in cortical bone, marrow, and muscle in canine hind leg by femoral artery catheterization. *Calcified Tissue International* 14: 301–307, 1974.

31. H.Sugimoto, W.W. Monafo. Regional Blood Flow in Sciatic Nerve, Biceps Femoris Muscle, and Truncal Skin in Response to Hemorrhagic Hypotension. *J Trauma* 27: 1025–1030, 1987.

32. J-M. R. Detry, G. L. Brengelmann, L. B. Rowell, C. Wyss. Skin and muscle components of forearm blood flow in directly heated man. *J Appl Physiol* 32: 506–511, 1972.

33. M. B. Ducharme, P. Tikuisis. Role of blood as heat source or sink in human limbs during local cooling and heating. *J Appl Physiol* 76: 2084–2094, 1994.

34. K. Yue, X. Zhang, F. Yu. Simultaneous estimation of thermal properties of living tissue using noninvasive method. *Int J Thermophysics* 28: 1470–1489, 2007.

35. B. L. Bullock, P. P. Rosendahl. *Pathophysiology, Adaptations and Alteration in Function.* Philadelphia: Lippincott, 1992.

36. P. Tikuisis, M. B. Ducharme. Finite-element solution of thermal conductivity of muscle during cold water immersion. *J Appl Physiol* 70: 2673–2681, 1991.

37. J. Harris, F. Benedict. A biometric study of human basal metabolism, *Proc Natl Acad Sci USA* 4: 370–373, 1918.

38. D. H. Silverthorn. *Human Physiology, An Integrated Approach*. New Jersey: Prentice-Hall, 2001.

39. C. K. Charny. Mathematical models of bio-heat transfer. In: *Advances in Heat Transfer*, edited by Cho YI. New York: Academic, 19–155, 1992.

40. S. W. Chang. Effect of Local Hyperthermia on Blood Flow and Microenvironment: A Review. *Cancer Res* 44: 4721s–4730s, 1984.

41. D. E. Lemons, S. Chien, L. I. Crawshaw, S. Weinbaum, L. M. Jiji. Significance of vessel size and type in vascular heat transfer. *Am J Physiol Regul Integr Comp Physiol* 253: R128–R135, 1987.

42. M. Praprotnik, M. Šterk, R. Trobec. Inhomogeneous heat-conduction problems solved by a new explicit finite difference scheme. *J Pure and Applied Mathematics* 13: 275–291, 2004.

43. R. Trobec, B. Slivnik, B. Gersak, T. Gabrijelcic. Computer simulation and spatial modelling in heart surgery. *Comput Biol Med* 28: 393–403, 1998.

44. P. Bernardi, M. Cavagnaro, S. Pisa, E. Piuzzi. Specific absorption rate and temperature elevation in a subject exposed in the far-field of radio-frequency sources operating in the 10–900-MHz Range. *IEEE Trans Biomed Eng* 50: 295–304, 2003.

45. R. Trobec, M. Šterk, S. Almawed, M. Veselko. Computer simulation of topical knee cooling. *Comput Biol Med* 33: 1076–1083, 2008.

Author Biography

Roman Trobec received Ph.D. degree in electrical engineering from University of Ljubljana. He is a principal investigator at Jožef Stefan institute, Department of Communication Systems. He is associate professor at the Faculty of Electrical Engineering and Faculty of Computer and Information Science in Ljubljana and visiting professor in the field of High Performance Scientific Computing, at the University of Salzburg, Department of the Scientific Computing. His research interests covers parallel and distributed computing, signal processing, biomedical research, telemedicine, sensor networks, computer simulations and communication systems. He works on applied projects related to the design and development of computer networks, cluster computing, bio-signal analysis, and computer simulations.

Matjaž Depolli received B.Sc. in computer and information science from University of Ljubljana in 2005. He joined Jožef Stefan Institute, Department of Communication Systems as a young researcher the same year. He is a PhD student of New Media and E-science programme of Jožef Stefan International Postgraduate School. His research interests include evolutionary computation, parallel computing, artificial intelligence, biomedical research, sensor networks, and computer simulations.

Conflict of Interest Statement

None declared.